The Promise of Immuno-PET in Radioimmunotherapy

Iris Verel, PhD[1]; Gerard W.M. Visser, PhD[2]; and Guus A. van Dongen, MS, PhD[1]

[1]*Department of Otolaryngology/Head and Neck Surgery, VU University Medical Center, Amsterdam, The Netherlands; and*
[2]*Department of Nuclear Medicine and PET Research, VU University Medical Center, Amsterdam, The Netherlands*

Immuno-PET as a quantitative imaging procedure before or concomitant with radioimmunotherapy is an attractive option to improve confirmation of tumor targeting and especially assessment of radiation dose delivery to both tumor and normal tissues. General information about PET, PET systems, and quantification is provided in this review. The requirements for an appropriate positron emitter and characteristics of the most attractive candidate emitters for immuno-PET are discussed. An overview of preclinical and clinical immuno-PET studies reported in the literature is provided.

Key Words: immuno-PET; radioimmunotherapy; monoclonal antibodies; positron emitters; oncology

J Nucl Med 2005; 46:164S–171S

Cancer treatment with radioimmunotherapy (RIT), consisting of radionuclides coupled to monoclonal antibodies (mAbs), has been the focus of research for more than 2 decades. The concept that mAbs could maximize the targeting of radiation to tumors while minimizing dose delivery to normal tissues has proven its worth only in recent years. Currently, 2 RIT procedures, ^{90}Y-ibritumomab tiuxetan (Zevalin; IDEC Pharmaceuticals) and ^{131}I-tositumomab (Bexxar; Corixa Corp.) have received approval by the U.S. Food and Drug Administration, and several radioimmunoconjugates are entering advanced-stage clinical trials. Although RIT appears to be successful in treatment of hematologic cancer types, treatment of solid tumors remains a challenge.

Important issues complicating successful application of RIT are the small therapeutic window (with bone marrow being the dose-limiting organ) and interpatient variations in pharmacokinetics and tumor uptake of the radioimmunoconjugate. Most radioimmunoconjugates currently in use are administered with some level of dose adjustment based on the patient's body weight or body surface area. These dosing schemes, although easy to implement, do not address the often substantial physiologic variability in mAb pharmacokinetics and target antigen accessibility among patients.

Performing radioimmunoscintigraphy (RIS) with trace-labeled mAbs before RIT enables the confirmation of tumor targeting and estimation of radiation dose delivery to both tumor and normal tissues. This approach can be used for in vivo characterization of new RIT candidate mAbs, as well as for the selection of RIT candidate patients, as is routine in both the Zevalin and Bexxar treatment regimens. In the Zevalin treatment regimen, a tracer amount of ^{111}In-ibritumomab tiuxetan is administered 7 to 9 d before therapy with ^{90}Y-ibritumomab tiuxetan, to rule out patients with unfavorable biodistribution. Dosimetry results from this diagnostic procedure have not been shown to correlate with toxicity (*1*). The Bexxar treatment schedule consists of a dosimetric dose of ^{131}I-tositumomab followed by a therapeutic dose of the same conjugate within 7 to 14 d. Patient-specific doses are administered on the basis of the calculated total-body residence time of dosimetric ^{131}I-tositumomab (*2*).

Detection of the γ-ray–emitting radionuclides ^{111}In and ^{131}I involves planar imaging with a γ-camera or SPECT. These procedures, however, have intrinsic limitations with respect to quantification, primarily because of insufficient correction for scatter and partial absorption of γ-photons in tissue. Because of more accurate scatter and attenuation corrections, PET is better qualified for tracer quantification. In addition, PET provides better spatial and temporal resolution and sensitivity than SPECT.

IMMUNO-PET: IMAGING AND QUANTIFICATION

Immuno-PET is based on annihilation coincidence detection after labeling of a mAb or mAb fragment with a positron-emitting radionuclide. The emitted positron (a positively charged β-particle) will travel a distance of a few millimeters, depending on the initial positron energy and the density of the surroundings. After having lost its kinetic energy, combining with an electron leads to the so-called annihilation process, yielding 2 photons each with an energy of 511 keV emitted simultaneously in opposite directions (Fig. 1). After administration of a PET conjugate to a patient, the distribution of the compound is monitored by

Received Apr. 6, 2004; revision accepted Oct. 21, 2004.
For correspondence or reprints contact: Guus A. van Dongen, MS, PhD, Department of Otolaryngology/Head and Neck Surgery, VU University Medical Center, De Boelelaan 1117, P.O. Box 7057, 1007 MB Amsterdam, The Netherlands.
E-mail: gams.vandongen@vumc.nl

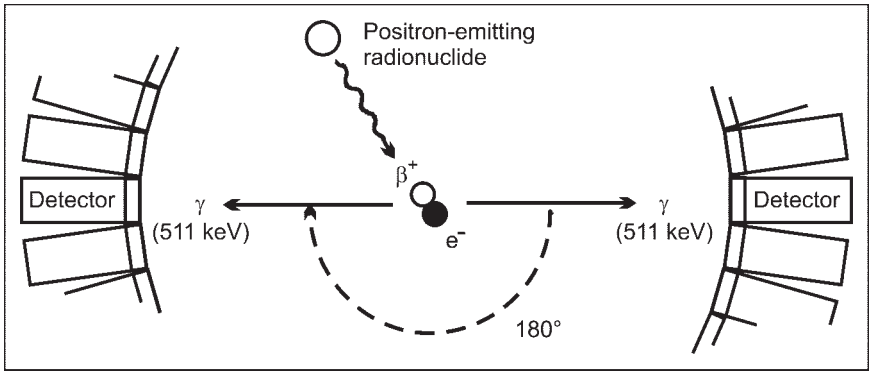

FIGURE 1. Positron emission, annihilation, and coincidence detection. Positron is emitted during decay of radionuclide, travels short distance, and combines with electron. Positron and electron annihilate, converting mass into 2 511-keV photons emitted at 180° to each other. Two annihilation photons are electronically detected as coincidence event when they strike opposing detectors simultaneously (detector ring schematically depicted).

detection of the annihilation photon pairs with a PET camera. A PET camera consists of a ring of detectors placed around the body of the patient. If 2 photons are registered by detectors on opposite sides of the body within a very short time, it is assumed that somewhere along the line between the 2 detectors an annihilation event has taken place. By calculating the crossing of all the lines of response (LORs), the location of the radiation source can be determined.

For dosimetry purposes, immuno-PET must provide reliable quantitative information. All photon pairs with energies that fall within the PET acquisition energy window (typically 350–650 keV) and that are detected in coincidence within a certain time period (coincidence time window, approximately 5–15 ns) are called coincidences. In addition to true coincidences, the gross coincidence rate can include scatter coincidences, random coincidences, and spurious true coincidences (Fig. 2). Spurious true coincidences can occur when an annihilation photon is registered together with an emitted single γ-photon from the same decay event (prompt γ-photon) and with an energy that falls within the PET acquisition energy window. In contrast to scatter and random coincidences, the occurrence of spurious true coincidences depends on the positron emitter used. For all 3, however, the LOR is not representative of the annihilation location and degrades the image quality. In addition, some portion of the annihilation photons will not be detected as a result of attenuation and dead time. Attenuation is the loss of true coincidences through Compton processes and absorption within tissue, causing 1 or both of the annihilation photons to fall outside the PET acquisition energy window or coincidence time window. The probability of a true coincidence detection is the product of the probabilities of each of the 2 annihilation photons escaping the body without interaction. For this reason, the amount of attenuation along a specific LOR is the same, independent of the location of the event on the LOR. This holds true even if the event took place outside the body. This fact is used in attenuation correction and requires an additional transmis-

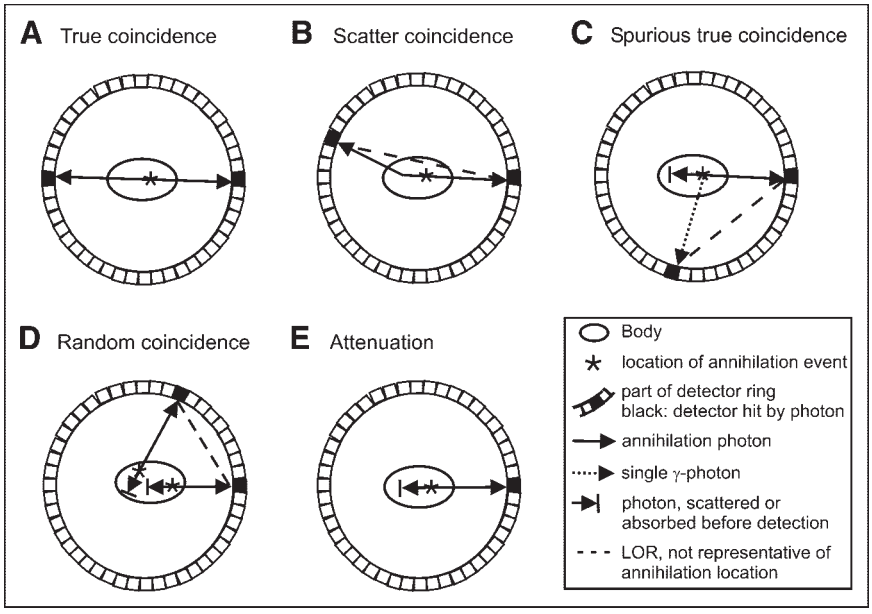

FIGURE 2. (A) True coincidence. Two annihilation photons, emitted from same annihilation event, travel in opposite directions without interaction with body, and are detected by opposing detectors. (B) Scatter coincidence. One photon from annihilation travels without interaction, and other annihilation photon is deflected because of scattering in body. (C) Spurious true coincidence. Single γ-photon is detected simultaneously with annihilation photon (or another single γ-photon), both emitted from same decay event. (D) Random coincidence. Two annihilation photons (or single γ-photons) emitted from 2 separate decay events are detected by chance within coincidence time window. (E) Attenuation. One (or both) annihilation photons is (are) not detected as result of scattering or absorption within body. In scatter, spurious, and random coincidences, LOR drawn between 2 detectors is not representative of annihilation location (B–D). Three or more photons (multiples) detected in coincidence are rejected by PET coincidence electronics.

sion scan in which the body is scanned with a rotating external radioactive point or line source. Dead time losses result from the system's inability to process an infinite number of photons at the same time. Dead time losses can be minimized by using a system with many independent detectors, fast scintillators, and fast processing electronics. To arrive at a quantitative image, the raw PET data must be corrected for the aforementioned disturbing effects.

After correction of raw PET data, the only factor influencing quantitative PET analysis of radioactivity is resolution related. Because of limited spatial resolution, the spread of locoregional radioactivity to surrounding areas must be considered. With small objects, the true radioactivity concentration of a hot object in cold surroundings will be underestimated in the PET image, whereas that of a cold object in hot surroundings will be overestimated (Fig. 3). The loss of radioactivity from the object into the surroundings and the contribution of near-surrounding spillover radioactivity into the object are called partial-volume effects. These partial-volume effects can be corrected for when the correction factors are known from test measurements and if the true volume of the object is known by anatomic imaging (*3,4*). Quantitative imaging in immuno-PET is challenging because of the relatively low object (e.g., tumor)-to-background radioactivity uptake ratios.

DEVELOPMENT IN CLINICAL PET IMAGING SYSTEMS

In 1975, the first PET scanner with thallium-doped sodium iodide (NaI[Tl]) detectors that could form true tomographic images was developed by Phelps et al. (*5*). Since then, the PET scanner has undergone several developments with respect to scintillation crystals and system design.

Over the years, the hexagonal and octagonal designs of the first PET systems were followed by circular designs.

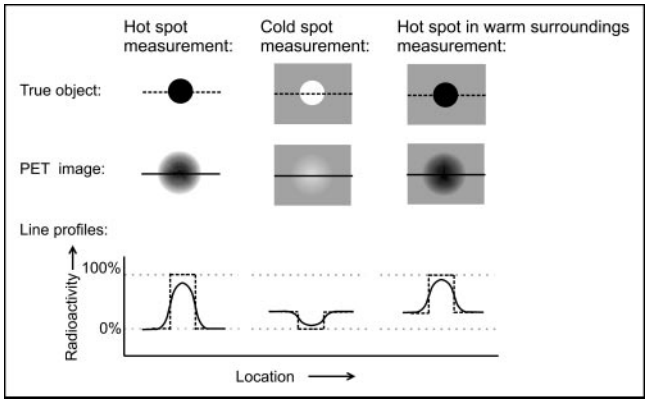

FIGURE 3. Schematic presentation of partial-volume effects. Slices through center of true and PET-imaged object (i.e., a sphere) and corresponding line profiles (dashed line = true object; solid line = PET image) for 3 conditions of radioactivity distribution: only object filled with radioactivity (hot spot), only surroundings filled with radioactivity (cold spot), or object filled with higher concentration of radioactivity than surroundings (hot spot in warm surroundings).

Today, most PET scanners contain bismuth germanate as scintillation material because of its greater efficiency for detecting 511-keV photons (*6*). In recent years, 2 promising new scintillation crystals, cerium-doped gadolinium oxyorthosilicate and cerium-doped lutetium oxyorthosilicate, have been applied in PET scanners, and several other detector materials are under investigation. It is expected that advances in this area will further improve PET sensitivity and resolution (*7*).

To facilitate accurate interpretation of PET images and dosimetry, it has been proposed that PET be combined with anatomic imaging by CT or MR imaging to provide simultaneous registration of both biologic function and anatomy. In only a few years, hybrid PET/CT scanners were developed and marketed commercially and now account for more than 65% of all PET sales. An extensive description of the current state of PET/CT has been published (*8*). Although combining PET with MR imaging is technologically more challenging because of the strong magnetic fields restricting the use of certain electronic components, the first MR imaging-compatible PET scanner has been developed. The availability of anatomic data not only provides landmarks for PET image interpretation but also can be used for attenuation correction, reduction of image noise, and partial volume correction.

POSITRON EMITTERS FOR IMMUNO-PET

For a positron emitter to be appropriate for immuno-PET, several aspects must be considered. The applicability of a positron emitter is dependent on the availability of methods to obtain it in pure and sufficient amounts, the time period available for transportation and labeling, the availability of procedures for its stable coupling to the mAb with maintenance of the antibody's in vivo biodistribution characteristics, and identification of undesirable components in its decay scheme that could compromise image quality and quantification accuracy. The predominant factor for determining a positron emitter's suitability for immuno-PET is its physical half-life. This must be compatible with the time needed for a mAb or mAb fragment to achieve optimal tumor-to-nontumor ratios (typically 2–4 d for intact mAbs and 2–6 h for mAb fragments). Thus far, radiolabeled intact mAbs have been used in tumor detection and treatment planning, as well as in RIT, whereas the application of mAb fragments has been restricted for the most part to tumor detection. Although the use of shorter-lived positron emitters (with half-lives of hours) for immuno-PET with mAb fragments is an option, the kinetics of intact mAbs demand the use of long-lived positron emitters (half-lives of days) to allow imaging at later time points for obtaining maximum information.

Given these considerations, the application of positron emitters with half-lives of minutes, such as the bioradionuclides ^{15}O, ^{13}N, and ^{11}C, is out of the question. The positron emitters that have been evaluated in preclinical and clinical

TABLE 1
Decay Characteristics of Positron Emitters Used in Preclinical or Clinical Radioimmunoscintigraphy Studies*

Positron emitter	Production	Half-life (h)	Main β^+-energies† (keV)‡	(%)	Main γ-energies† (keV)	(%)	Intrinsic spatial resolution loss§ (mm)	Reference
^{94m}Tc	^{94}Mo(p,n)	0.87	2,438	67.6	871	88.5	3.2	(*9,10*)
					1,869	5.4		
^{68}Ga	^{68}Ga/^{68}Ga generator	1.13	1,899	87.9	—		2.4	(*11*)
^{18}F	^{18}O(p,n) ^{20}Nc(d,α)	1.83	634	100.0	—		0.7	(*12*)
^{64}Cu	^{64}Ni(d,2n) ^{64}Ni(p,n)	12.7	653	17.9	—		0.7	(*11,13*)
^{86}Y‖	^{86}Sr(p,n)	14.7	1,221	12.5	443	16.9	1.8	(*14–16*)
			1,545	5.6	628	32.6		
					646	9.2		
					703	15.4		
					777	22.4		
					1,077	82.5		
					1,153	30.5		
					1,854	17.2		
					1,921	20.8		
^{76}Br‖	^{75}As(^{3}He,2n)	16.2	871	5.9	559	72.3	5.3	(*17*)
	^{76}Se(p,n)		990	5.1	657	15.5		
			3,382	27.6	1,216	8.7		
			3,941	6.0	1,854	14.0		
					2,793	5.3		
					2,951	7.6		
^{89}Zr	^{89}Y(p,n)	78.4	897	22.7	909	99.9	1.0	(*4,18*)
^{124}I‖	^{124}Te(p,n)	100.3	1,535	11.2	603	62.9	2.3	(*19,20*)
	^{124}Te(d,2n)		2,138	11.2	723	10.1		
	^{125}Te(p,2n)				1,691	10.6		

*Half-life, main β^+-energy keV and percentage; and main γ-energy keV and percentage as reported by International Commission on Radiological Protection (*21*) and the NuDat database (*22*).
†Only energies ≥5% are given.
‡Maximum β^+-energy.
§Calculated according to Pagani et al. (*11*).
‖Positron emitter with more than 50 γ-energies.

immuno-PET studies are listed in Table 1. On the basis of their half-lives, most of these radionuclides are better suited for use in combination with mAb fragments (in particular ^{94m}Tc, ^{68}Ga and ^{18}F, and, to a lesser extent, ^{64}Cu, ^{86}Y, and ^{76}Br). The 2 positron emitters that are suitable for imaging of mAb fragments as well as intact mAbs are ^{124}I and ^{89}Zr. The half-lives of these radionuclides offer an advantage with respect to the logistics of radiolabeling and transportation but a potential disadvantage with respect to the radiation burden to the patient, especially when coupled to compounds with long biologic half-lives, such as intact mAbs. This disadvantage might be overcome by the introduction of the latest generation of high-resolution PET scanners with higher sensitivity, allowing lower doses of injected radioactivity for comparable images.

Other aspects of a positron emitter to be considered are the presence of prompt single γ-photons causing spurious true coincidences (^{86}Y, ^{76}Br, and ^{124}I), high β^+-energy resulting in an intrinsic resolution loss (^{94m}Tc, ^{68}Ga, ^{76}Br, and ^{124}I), and the presence of radionuclidic impurities or radioisotopes of the same element generated during cyclotron production (^{94m}Tc and ^{64}Cu). Except for the production of ^{76}Br and ^{89}Zr, all positron emitters listed in Table 1 require enrichment of the target material, a process that is expensive while 100% enrichment is never reached. The positron emitters ^{68}Ga, ^{18}F, ^{64}Cu, ^{86}Y, and ^{89}Zr need indirect labeling methods with bifunctional chelates, but ^{94m}Tc, ^{76}Br, and ^{124}I can also be coupled directly to mAbs.

EXPERIENCES WITH IMMUNO-PET

Although several positron emitters have been suggested for mAb labeling, immuno-PET research is still in its infancy. Most immuno-PET studies have focused on animal models, and clinical evaluations are rare. This is mainly the result of the limited availability of suitable positron emitters, a lack of robust labeling methods, and, until recently, the relatively small number of PET cameras in operation.

An application that shows considerable potential is the use of quantitative PET in combination with RIT. For this purpose, the radioimmunoconjugates used for immuno-PET and RIT should demonstrate a similar biodistribution, and, therefore, radionuclides (and, if required, chelates) with comparable chemical properties must be chosen.

Because PET is believed to be superior to SPECT with respect to quantification, several PET radioisotopes have been suggested as substitutes for γ-emitting radionuclides used in RIS. At least in theory, this could enable easy conversion from a SPECT to a PET procedure. Examples of PET/SPECT radioisotope pairs are ^{94m}Tc/^{99m}Tc, ^{67}Ga/^{68}Ga, and ^{124}I/^{123}I, and examples of PET/RIT radioisotope pairs are ^{64}Cu/^{67}Cu, ^{86}Y/^{90}Y, and ^{124}I/^{131}I. However, PET/RIT surrogate pairs also can be considered, such as ^{94m}Tc/^{186}Re, ^{94m}Tc/^{188}Re, ^{124}I/^{186}Re, ^{124}I/^{188}Re, ^{76}Br/^{131}I, and ^{89}Zr/^{90}Y.

At the present time, ^{18}F-FDG is by far the most widely available and most widely applied clinical PET tracer. The application of ^{18}F in immuno-PET, however, is limited to mAb fragments because of the tracer's short half-life (1.83 h). Although several conjugates have been evaluated in biodistribution studies in xenograft-bearing mice, no quantitative preclinical or clinical PET studies have been performed (*23,24*).

Other short-lived positron emitters are ^{94m}Tc and ^{68}Ga. The imaging agent carcinoembryonic antigen (CEA)-scan, supplied as an instant kit containing lyophilized NP-4 F(ab′) for labeling with ^{99m}Tc, has been used for coupling to ^{94m}Tc instead (*25*). Although ^{94m}Tc and ^{99m}Tc are isotopes of the same element, labeling results were different because NP-4 F(ab′) contained much more reoxidized NP-4 F(ab′)$_2$ as a result of ^{94m}Tc labeling. No in vivo evaluation of these conjugates was performed. ^{68}Ga coupled to small mAb fragments or for use in so-called pretargeting strategies has been investigated. Pretargeted PET with ^{68}Ga has been evaluated in mice bearing CD44v6- and MUC1-expressing tumors and in patients with breast cancer (*26,27*). In the latter study, patients received anti-MUC1/anti-Ga-chelate bispecific antibody (Bs-mAb), followed 18 h later by a blocker to remove residual circulating Bs-mAb from the blood and another 15 min later by the chelate labeled with 230–300 MBq ^{68}Ga. PET was started 60–90 min after injection of the ^{68}Ga-chelate. In 10 patients, 14 of 17 known breast lesions, ranging from 10 to 80 mm in size, were clearly visualized with PET as foci with increased activity. No false-positive readings were obtained. Detection of axillary lymph node metastases was hampered by a high activity in blood vessels near the lymph nodes. It was concluded that PET offered better sensitivity for the detection of breast cancer at low tumor contrast than conventional RIS.

Smith-Jones et al. (*28*) have demonstrated the potential of ^{68}Ga-immuno-PET for quantitative imaging of HER2 expression modulation. Tumor-bearing mice were treated with 17-allylaminogeldanamycin, a heat shock protein 90 inhibitor that causes degradation of the HER2 receptor. A ^{68}Ga-labeled F(ab′)$_2$ fragment of the anti-HER2 antibody herceptin was used for PET of HER2 expression. A linear correlation (R^2 = 0.97) was found between tracer uptake quantified by direct assessment of resected tumors by γ-counter and tracer uptake estimated by PET.

Positron emitters suggested for immuno-PET with half-lives of several hours (but less than 1 d) are ^{64}Cu, ^{86}Y, and ^{76}Br. ^{64}Cu has been coupled to the intact anticolorectal murine mAb 1A3 for immuno-PET in patients with suspected advanced primary or metastatic colorectal cancer (*29*). After injection of the conjugate (5–20 mg mAb; 370 MBq), PET was performed once or twice (at 4 h or at 4 and 36 h). All 36 patients entered in this study underwent CT or MR imaging, and 18 patients were also studied with ^{18}F-FDG PET. In 29 patients, 1 or more tumor sites (40 of 56 total) were identified on immuno-PET, absence of tumor was confirmed in 5 patients, and tumor status was not confirmed in 2 patients. All 17 primary and recurrent sites were clearly visualized, but only 23 of 39 metastatic sites (59%) were detected. The sensitivity of immuno-PET was best in abdomen and pelvis. In these regions 11 occult small tumor lesions were detected, including 9 small foci <2 cm in diameter that were not detected by CT or MR imaging. For detection of abdominal–pelvic tumors, immuno-PET exhibited better sensitivity than CT or MR imaging, and appeared as sensitive as ^{18}F-FDG PET. In contrast, detection of metastatic disease of liver and lung was difficult because of high blood-pool activity at the early imaging time points, which were chosen because of the half-life of ^{64}Cu (12.7 h). Detection of liver metastases was also hampered by nontarget background activity, caused by ^{64}Cu residualizing in the liver after catabolism of the conjugate.

In another study, the genetically engineered anti-CEA T84.66/GS18 minibody was labeled with ^{64}Cu via the 1,4,7,10-tetraazacyclododecane-*N,N′,N″,N‴*-tetraacetic acid (DOTA) chelate, and PET of colorectal carcinoma xenograft–bearing nude mice was performed (*30*). Tumors of 25–395 mg were visualized within a few hours after injection of the tracer. With these ^{64}Cu-conjugates high retention of activity in the liver was also observed, resulting in tumor-to-liver uptake ratios <1. Such retention would restrict the detection of hepatic lesions. ^{64}Cu has also been used in a pretargeting strategy, consisting of the antiepithelial cell adhesion molecule mAb NR-LU-10 conjugated with streptavidin and a ^{64}Cu-DOTA-biotin ligand (*31*). In mice bearing colorectal carcinoma xenografts, a maximum tumor uptake was reached with this strategy at 1 h after injection. The tumor-to-blood ratio of areas under the curve was 14 times higher for pretargeted ^{64}Cu-DOTA-biotin than for conventionally labeled ^{64}Cu-DOTA-NR-LU-10. Although no PET was performed in this study, superior PET contrast might be expected when using the pretargeting strategy. Also in this study, increased uptake of ^{64}Cu in the liver was observed, but uptake levels were much lower than in tumor.

The positron emitter ^{86}Y has been coupled to the anti-Lewis Y humanized mAb (hMAb) hu3S193 and the anti-HER2 hMAb herceptin, and their biodistributions were compared with those of their respective ^{111}In-labeled mAbs (*15,32*). The rational for this comparison was that PET with ^{86}Y-mAb might be better qualified for predicting ^{90}Y-mAb localization and dose delivery in RIT studies than ^{111}In-mAb SPECT. Although biodistribution data from both studies indicated that this might be the case, accurate quantitation of ^{86}Y with PET still remains a challenge because of the prompt single γ-photons emitted by this positron emitter (*32*). ^{76}Br has been coupled to the anti-CEA mAb 38S1 by Lövqvist et al. (*33*), and biodistribution studies and PET were performed in colon carcinoma xenograft–bearing nude rats. The authors hypothesized that ^{76}Br might be an interesting alternative to ^{124}I as a PET radionuclide substitute for the iodine radioisotopes used in RIS and RIT. To this end, ^{76}Br-38S1 and ^{125}I-38S1 were prepared by direct labeling, and their biodistribution compared in nude rats carrying human colon xenografts. Although all tumors could be identified readily by PET, the concentrations of ^{76}Br radioactivity in tumor, blood, and normal tissues were higher than corresponding ^{125}I concentrations at all time points. This was mainly the result of catabolism of radiolabeled mAb, resulting in free radiohalides, of which $^{76}Br^-$ was retained in the blood pool in contrast to the rapidly excreted $^{125}I^-$ ion. These data suggest that ^{76}Br cannot be used as a PET radionuclide substitute for iodine radioisotopes.

^{124}I and ^{89}Zr are long-lived positron emitters. In the 1990s, several studies were performed with ^{124}I-labeled mAbs in animals and patients. Snook et al. (*34*) evaluated the biodistribution of ^{124}I-labeled H17E2 in HEp2 xenograft-bearing nude mice, without comparison with ^{131}I-labeled H17E2 and without performing PET. Similar studies were performed with ^{124}I-labeled rat mAb ICR12 for the targeting of human breast carcinoma xenografts overexpressing the c-erb B2 proto-oncogene product (*35*). PET was performed (but without quantitative analyses), and tumor xenografts of 6-mm diameter were successfully delineated with high resolution at 24, 48, and 120 h after injection. Clinical immuno-PET studies with ^{124}I-labeled mAbs have been performed in only a small numbers of patients (*36,37*). Wilson et al. (*37*) used PET with ^{124}I-labeled mMAb HMFG1 for tumor detection in 7 breast cancer patients and for quantitative measurement of conjugate uptake in tumors. In only 2 of 7 patients the tumor uptake of the specific antibody was higher than that seen with the nonspecific antibody, and therefore mMAb HMFG1 was not further studied in immuno-PET. After almost a decade, interest in ^{124}I-labeled mAbs has been renewed. The complementarity-determining region grafted hMAb A33 was labeled with ^{124}I, and colon xenograft-bearing mice were imaged (*38*). Biodistribution studies revealed excellent tumor uptake of 50.0 ± 0.7 %ID/g, with maximum uptake at 4 d after injection. PET detected antigen-positive tumors (range, 0.2–0.7 g) by 4 h after injection, and high-resolution images were obtained by 24 h after injection. In these studies, PET was not exploited for quantitative measurements. The potential of ^{124}I-labeled genetically engineered antibody fragments for tumor detection was confirmed by Sunderesan et al. (*39*), who demonstrated high resolution images and specific localization (compared with ^{18}F-FDG) with anti-CEA T84.66 minibody and diabody in nude mice bearing colon carcinoma xenografts. The potential of ^{124}I-labeled mAbs for pretherapy PET was demonstrated by Verel et al. (*40*). To this end, the scouting performance of ^{124}I-labeled chimeric mAb (cMAb) U36 was evaluated in a biodistribution experiment on coinjection with ^{131}I-labeled cmAb U36, and by PET in nude mice bearing head and neck cancer xenografts. ^{124}I- and ^{131}I-labeled cmAb U36 produced fully concordant tissue uptake values, whereas selective tumor uptake was confirmed with immuno-PET with visualization of all 15 tumors.

Recently, the positron emitter ^{89}Zr has been coupled to cmAb U36 via the bifunctional derivative of the chelate desferrioxamine B, and the in vivo behavior of the conjugate was evaluated by biodistribution and PET studies in nude mice bearing head and neck cancer xenografts (*18*). These studies demonstrated selective tumor targeting of ^{89}Zr-labeled cmAb U36 and visualization of small tumors in the range of 19–154 mg on PET images (Fig. 4). To

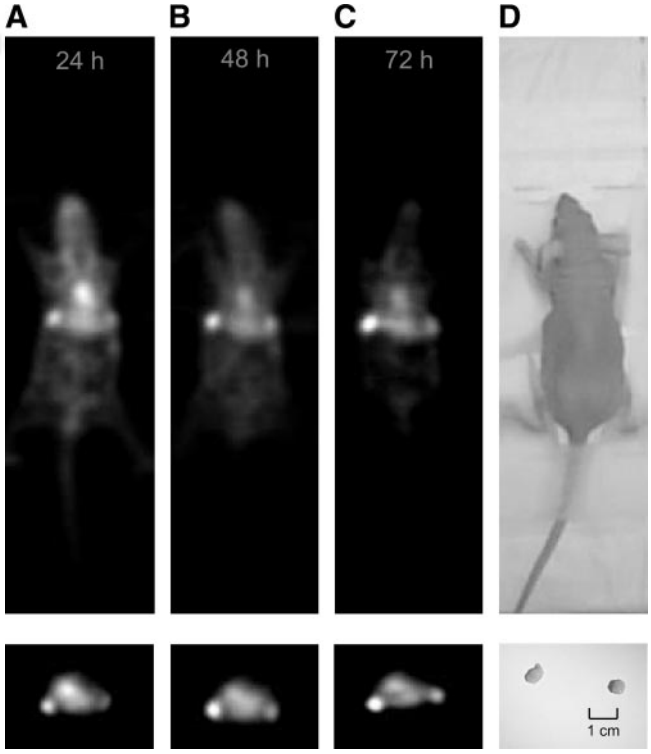

FIGURE 4. Head and neck cancer xenograft–bearing nude mouse injected with cmAb U36-*N*-sucDf-^{89}Zr (100 μg of mAb; 3.7 MBq). Coronal (upper) and transaxial (lower) PET images were obtained from same mouse at 24 (A), 48 (B), and 72 h (C). Image planes are those for which both tumors of same animal were visible. (D) Photographs of imaged mouse and excised tumors (left, 47 mg; right, 45 mg).

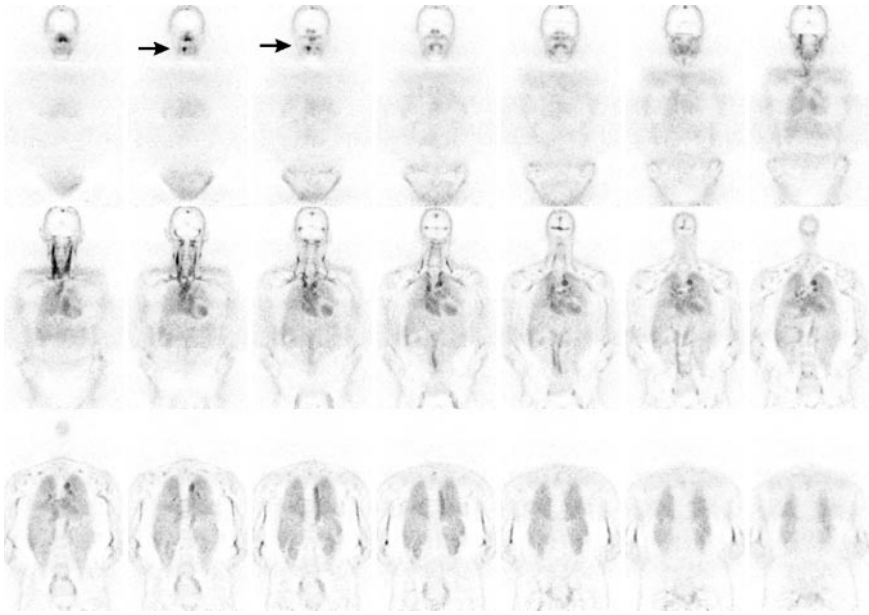

FIGURE 5. ECAT EXACT HR+ PET coronal images of patient with head and neck cancer (T2N0) 24 h after injection of cmAb U36-*N*-sucDf-^{89}Zr. Increased uptake is seen in primary tumor at right side of tongue (arrow). Note high blood-pool activity at this early time point.

examine the applicability of ^{89}Zr-labeled mAb as a scouting procedure for ^{90}Y-mAb RIT, cmAb U36 was labeled with ^{89}Zr and ^{88}Y (as substitute for ^{90}Y) (*4*). The radioimmunoconjugates were coinjected in xenograft-bearing nude mice, and biodistribution was determined at 3, 24, 48, 72, and 144 h after injection. The radioimmunoconjugates showed similar uptake in tumor, blood, and other organs, except for sternum and thigh bone at later time points. Small differences were found in kidney and liver. Quantitative imaging performance of ^{89}Zr approximated that of ^{18}F, whereas, after correction for partial-volume effects, a good correlation was found between image-derived ^{89}Zr tumor radioactivity and γ-counter ^{89}Zr radioactivity values of excised tumors (R^2 = 0.79). These data are in line with the previously discussed data of Smith-Jones et al. (*28*) and confirm the accuracy of PET for noninvasive estimation of mAb tissue accumulation. Because of the encouraging results obtained with ^{89}Zr immuno-PET, ^{89}Zr-labeled cmAb U36 is currently being evaluated for its capacity to detect primary tumors and metastases in patients with operable head and neck small-cell cancer. Preliminary data showed that tumor deposits can be visualized clearly after administration of 74 MBq ^{89}Zr (Fig. 5). A smooth interpretation of images, however, is hampered by high activity in blood vessels resulting from the long residence time of intact mAbs. To deal with this problem, combining immuno-PET with anatomic imaging seems an interesting future approach.

CONCLUSION

Immuno-PET combines the high resolution and quantitative aspects of PET with the high specificity and selectivity of mAbs. This makes immuno-PET an attractive imaging modality for tumor detection. Moreover, immuno-PET has the potential to supersede γ-camera imaging in combination with RIT, because it enables the sensitive confirmation of tumor targeting and a more reliable estimation of radiation dose delivery to both tumor and normal tissues. Improved assessment of mAb biodistribution permits the optimization of RIT (and other antibody-based therapies), as well as the individualization of RIT with respect to dose planning and selection of patients with the best chance to benefit from RIT.

ACKNOWLEDGMENTS

This study was supported by grants from the European Union FP6, LSHC-CT-2003–5032, STROMA. The publication reflects only the authors view. The European Commission is not liable for any use that may be made of the information contained.

REFERENCES

1. Wiseman GA, Kornmehl E, Leigh B, et al. Radiation dosimetry results and safety correlations from ^{90}Y-ibritumomab tiuxetan radioimmunotherapy for relapsed or refractory non-hodgkin's lymphoma: combined data from 4 clinical trials. *J Nucl Med.* 2003;44:465–474.
2. Wahl RL. The clinical importance of dosimetry in radioimmunotherapy with tositumomab and iodine I-131 tositumomab. *Semin Oncol.* 2003;30:31–38.
3. Geworski L, Knoop BO, de Cabrejas ML, Knapp WH, Munz DL. Recovery correction for quantitation in emission tomography: a feasibility study. *Eur J Nucl Med.* 2000;27:161–169.
4. Verel I, Visser GWM, Boellaard R, et al. Quantitative ^{89}Zr immuno-PET for in vivo scouting of ^{90}Y-labeled monoclonal antibodies in xenograft-bearing nude mice. *J Nucl Med.* 2003;44:1663–1670.
5. Phelps ME, Hoffman EJ, Mullani NA, Ter-Pogossian MM. Application of annihilation coincidence detection to transaxial reconstruction tomography. *J Nucl Med.* 1975;16:210–224.
6. Melcher CL. Scintillation crystals for PET. *J Nucl Med.* 2000;41:1051–1055.
7. Humm JL, Rosenfeld A, Del Guerra A. From PET detectors to PET scanners. *Eur J Nucl Med Mol Imaging.* 2003;30:1574–1597.
8. Czernin J, Schelbert H. PET/CT imaging: facts, opinions, hopes, and questions. *J Nucl Med.* 2004;45(suppl):1S–3S.
9. Qaim SM. Production of high purity ^{94m}Tc for positron emission tomography studies. *Nucl Med Biol.* 2000;27:323–328.

10. Smith MF, Daube-Witherspoon ME, Plascjak PS, et al. Device-dependent activity estimation and decay correction of radionuclide mixtures with application to Tc-94m PET studies. *Med Phys.* 2001;28:36–45.
11. Pagani M, Stone-Elander S, Larsson SA. Alternative positron emission tomography with non-conventional positron emitters: effects of their physical properties on image quality and potential clinical applications. *Eur J Nucl Med.* 1997;24:1301–1327.
12. Glaser M, Luthra SK, Brady F. Applications of positron-emitting halogens in PET oncology. *Int J Oncol.* 2003;22:253–267.
13. McCarthy DW, Shefer RE, Klinkowstein RE, et al. Efficient production of high specific activity ^{64}Cu using a biomedical cyclotron. *Nucl Med Biol.* 1997;24:35–43.
14. Rösch F, Qaim G, Stöcklin G. Production of the positron emitting radioisotope ^{86}Y for nuclear medical applications. *Appl Radiat Isot.* 1993;44:677–681.
15. Garmestani K, Milenic DE, Plascjak PS, Brechbiel MW. A new and convenient method for purification of ^{86}Y using a Sr(II) selective resin and comparison of biodistribution of ^{86}Y and ^{111}In labeled herceptin. *Nucl Med Biol.* 2002;29:599–606.
16. Walrand S, Jamar F, Mathieu I, et al. Quantitation in PET using isotopes emitting prompt single gammas: application to yttrium-86. *Eur J Nucl Med.* 2003;30:354–361.
17. Lubberink M, Schneider H, Bergstrom M, Lundqvist H. Quantitative imaging and correction for cascade gamma radiation of ^{76}Br with 2D and 3D PET. *Phys Med Biol.* 2002;47:3519–3534.
18. Verel I, Visser GWM, Boellaard R, Stigter-Van Walsum M, Snow GB, Van Dongen GAMS. ^{89}Zr immuno-PET: comprehensive procedures for the production of ^{89}Zr-labeled monoclonal antibodies. *J Nucl Med.* 2003;44:1271–1281.
19. Pentlow KS, Graham MC, Lambrecht RM, et al. Quantitative imaging of iodine-124 with PET. *J Nucl Med.* 1996;37:1557–1562.
20. Herzog H, Tellmann L, Qaim SM, Spellerberg S, Schmid A, Coenen HH. PET quantitation and imaging of the non-pure positron-emitting iodine isotope ^{124}I. *Appl Radiat Isot.* 2002;56:673–679.
21. Sowby FD, ed. *Radionuclide Transformations: Energy and Intensity of Emissions.* International Commission on Radiological Protection Publication 38. Vol. 11–13. Oxford, UK: Pergamon Press; 1983:14, 74, 90, 144, 202, 218, 249, 444.
22. Kinsey RR, ed. *The NuDat Program for Nuclear Data on the Web.* Version 2.5. Available at: http://www.nndc.bnl.gov/nndc/nudat/. Accessed September 1, 2004.
23. Garg PK, Garg S, Bigner DD, Zalutsky MR. Localization of fluorine-18-labeled Mel-14 monoclonal antibody $F(ab')_2$ fragment in a subcutaneous xenograft model. *Cancer Res.* 1992;52:5054–5060.
24. Choi CW, Lang L, Lee JT, et al. Biodistribution of ^{18}F- and ^{125}I-labeled anti-Tac disulfide-stabilized Fv fragments in nude mice with interleukin 2 alpha receptor-positive tumor xenografts. *Cancer Res.* 1995;55:5323–5329.
25. Griffiths GL, Goldenberg DM, Roesch F, Hansen HJ. Radiolabeling of an anti-carcinoembryonic antigen antibody Fab′ fragment (CEA-scan) with the positron-emitting radionuclide Tc-94m. *Clin Cancer Res.* 1999;5:3001s–3003s.
26. Klivényi G, Schuhmacher J, Patzelt E, et al. Gallium-68 chelate imaging of human colon carcinoma xenografts pretargeted with bispecific anti-CD44V6/anti-gallium chelate antibodies. *J Nucl Med.* 1998;39:1769–1776.
27. Schuhmacher J, Kaul S, Klivényi G, et al. Immunoscintigraphy with PET: Ga-68 chelate imaging of breast cancer pretargeted with bispecific anti-MUC1/anti-Ga chelate antibodies. *Cancer Res.* 2001;61:3712–3717.
28. Smith-Jones PM, Solit DB, Akhurst T, Afroze F, Rosen N, Larson SM. Imaging of the pharmacodynamics of HER2 degradation in response to Hsp90 inhibitors. *Nat Biotechnol.* 2004;22:701–706.
29. Philpott GW, Schwarz SW, Anderson CJ, et al. RadioimmunoPET: detection of colorectal carcinoma with positron-emitting copper-64-labeled monoclonal antibody. *J Nucl Med.* 1995;36:1818–1824.
30. Wu AM, Yazaki PJ, Tsai S, et al. High-resolution microPET imaging of carcinoembryonic antigen-positive xenografts by using a copper-64-labeled engineered antibody fragment. *Proc Natl Acad Sci USA.* 2000;97:8495–8500.
31. Lewis MR, Wang M, Axworthy DB, et al. In vivo evaluation of pretargeted ^{64}Cu for tumor imaging and therapy. *J Nucl Med.* 2003;44:1284–1292.
32. Lövqvist A, Humm JL, Sheikh A, et al. PET imaging of ^{86}Y-labeled anti-Lewis Y monoclonal antibodies in a nude mouse model: comparison between ^{86}Y and ^{111}In radiolabels. *J Nucl Med.* 2001;42:1281–1287.
33. Lövqvist A, Sundin A, Alström H, Carlsson J, Lundqvist H. Pharmacokinetics and experimental PET imaging of a bromine-76-labeled monoclonal anti-CEA antibody. *J Nucl Med.* 1997;38:395–401.
34. Snook DE, Rowlinson-Busza G, Sharma HL, Epenetos AA. Preparation and in vivo study of ^{124}I-labelled monoclonal antibody H17E2 in a human tumour xenograft model. A prelude to positron emission tomography (PET). *Br J Cancer* 1990;10(suppl):89–91.
35. Westera G, Reist HW, Buchegger F, et al. Radioimmuno positron emission tomography with monoclonal antibodies: a new approach to quantifying in vivo tumour concentration and biodistribution for radioimmunotherapy. *Nucl Med Commun.* 1991;12:429–437.
36. Larson SM, Pentlow KS, Volkow ND, et al. PET scanning of iodine-124–3F8 as an approach to tumor dosimetry during treatment planning for radioimmunotherapy in a child with neuroblastoma. *J Nucl Med.* 1992;33:2020–2023.
37. Wilson CB, Snook DE, Dhokia B, et al. Quantitative measurement of monoclonal antibody distribution and blood flow using positron emission tomography and ^{124}I in patients with breast cancer. *Int J Cancer.* 1991;47:344–347.
38. Lee FT, Hall C, Rigopoulos A, et al. Immuno-PET of human colon xenograft-bearing BALB/c nude mice using ^{124}I-CDR-grafted humanized A33 monoclonal antibody. *J Nucl Med.* 2001;42:764–769.
39. Sunderesan G, Yazaki P, Shively JE, et al. ^{124}I-labeled engineered anti-CEA minibodies and diabodies allow high-contrast, antigen-specific small-animal PET imaging of xenografts in athymic mice. *J Nucl Med.* 2003;44:1962–1969.
40. Verel I, Visser GWM, Vosjan MJWD, Finn R, Boellaard R, Van Dongen GAMS. High-quality ^{124}I-labelled monoclonal antibodies for use as PET scouting agents prior to ^{131}I-radioimmunotherapy. *Eur J Nucl Med Mol Imaging.* July 31, 2004. [Epub ahead of print.]

JNM The Journal of NUCLEAR MEDICINE

The Promise of Immuno-PET in Radioimmunotherapy

Iris Verel, Gerard W.M. Visser and Guus A. van Dongen

J Nucl Med. 2005;46:164S-171S.

The Journal of Nuclear Medicine is published monthly.
SNMMI | Society of Nuclear Medicine and Molecular Imaging
1850 Samuel Morse Drive, Reston, VA 20190.
(Print ISSN: 0161-5505, Online ISSN: 2159-662X)

SNMMI SOCIETY OF NUCLEAR MEDICINE AND MOLECULAR IMAGING